An experimental method to control pore structure in artificial conglomerate based on grain size distribution design

Authors: Wenbin Gao[1], Yiqiang Li[1], Huoxin Luan[2], Deng Pan[1], Xiangxing Xiang[2], and Han Cao[1],

[1]State Key Laboratory of Petroleum Resources and Prospecting, China University of Petroleum (Beijing), Beijing, China;

[2]Research Institute of Experimental and Testing, Xinjiang Oilfield Branch Company, PetroChina, Karamay, Xinjiang, China

Corresponding author: Yiqiang Li (yiqiangli@cup.edu.cn)

Key Points:

- An artificial conglomerate with wider pore distribution and more proportion of nano pores is developed by utilizing Portland cement as cementing agent
- Various features of pore structure, such as average radius and distribution morphology, are realized by adjusting grain size distribution
- Pore distribution morphology in artificial conglomerate has high similarity with natural cores in Karamay oilfield previously reported

Abstract

The conglomerate is characterized by multiscale grain packing structure and various pore distribution morphology, which is also named as multimodal structure. However, artificial conglomerate applying the experimental investigation differs significantly from natural conglomerates in terms of pore structure, due to centralized pore distribution and lack of nano-scale pores. Hence, we present an experimental method for controlling the pore structure in the artificial conglomerate. First of all, Portland cement was adopted as the main cementing agent, which could generate wider pore distribution and more proportion of nano-scale pores. Next, the grain size distribution design model was applied to realize the various pore structure. Finally, Genetic Programing was adopted to quantify the relationship between grain size distribution and pore structure. The results demonstrated that grain size distribution is composed of coarse grain peak (CGP) and fine grain peak (FGP), various morphology of grain distribution could be realized by adjusting the width and granularity of CGP and FGP. Moreover, lithology is determined by the average value μ_1 of CGP, while permeability is determined by the average value μ_2 of FGP. As the granularity difference between CGP and FGP performs larger, the morphology of pore distribution transforms from steep peak to hills in the conglomerate, most frequent and average radius of pore decrease, and capillary curve morphology transforms from concave to convex. In comparison with natural cores within alluvial fan of Karamay conglomerate reservoir, pore distribution morphology of artificial conglomerates has high similarity with natural cores.

1. Introduction

Compared with conventional sandstone, conglomerate performs as a distinctive sedimentary rock, composed predominantly of pre-existing rock fragments or clasts with a diameter greater than 2mm (Migoń, 2020). As a favorable reservoir for oil and gas, conglomerate has received worldwide attention due to an excellent exploration and development potential (Clarke, 1979; Gao et al., 2018; Kang et al., 2019; Liu et al., 2020; Yin, Chen, & Wu, 2018). Recently, abundant oil and gas resources have been recovered in the conglomerate reservoir in the Junggar Basin of China (Feng, Li, He, & Zheng, 2020; Yan et al., 2018; C. Zhang et al., 2020).

Normally, gravel, sandstone, and mud coexist in the conglomerate. Cavities formed among the gravel particles could be filled with fine particles such as sand or mud. Similarly, the pore space that has been filled might be filled again, which was deemed the multiscale packing structure. It's the complex packing structure that results in conglomerate possess more complex pore structure, a poorer correlation between porosity and permeability than conventional sandstone (Kang et al., 2019; Markussen, Dypvik, Hammer, Long, & Hammer, 2019; C. Zhang et al., 2020). The so-called "more complex pore structure" refers to broader pore-throat size distribution, ranging from 0.01 to 1000μm (Liu et al., 2020; Zhang, Wu, Zhong, & Shi, 2020) and more diversified pore-throat distribution morphology, such as unimodal, bimodal or multimodal (Mahmic, Dypvik, & Hammer, 2018; Senlin, Yukun, & Xiaojun, 2018; K. Zhang et al., 2020).

Due to the special pore structure, fluid flow characteristics in the conglomerate performed obviously different from sandstone. For instance, in the samples with similar permeability but the different modal distribution of pore-throat, conglomerate with multimodal pore-throat distribution has approximately three times shear rates than unimodal sandstone in the same velocity (Liu, Li, Lv, Li, & Chen, 2017). In the aspect of pore mobilization, mainly mobilized pores in SP flooding ranges from 1 to 3μm in the unimodal and bimodal sandstone, while the range of that concentrates on more than 3μm in the multimodal conglomerate (Liu et al., 2020). Therefore, the effect of pore structure on the research

regarding fluid flow in the complicated pore space definitely is of great significance(Jin et al., 2017; Qiang et al., 2020; Weichao et al., 2019).

Aim to investigate fluid flow characteristics, laboratory experiments are essential and necessary approach. Cores samples in the experiment have a significant influence on the research result. Plenty of scholars adopted outcrop, such as Berea and Bentheimer sandstone, to conduct flow characteristic research (Ebaga-Ololo & Chon, 2018; Kareem et al., 2017; Lin, Bijeljic, Pini, Blunt, & Krevor, 2018; Zhai et al., 2020). However, the outcrops in the former thesis were normally columnar cores with a diameter of 25 or 38mm. It's concluded that the size of the core samples has a considerable effect on the displacement efficiency, particularly in the conglomerate reservoir. Han and Liu (Han et al., 2018; Liu et al., 2020) demonstrated that full diameter long-core flooding experiment is more effective and closer to realistic reservoir percolation characteristics. Moreover, the swept efficiency of enhanced oil recovery (EOR) could be better reflected in the plane artificial core (Ma, Hou, Zhao, & Song, 2018; F. Zhao et al., 2018). Therefore, outcrops with large sizes are rare and difficult to obtain the desired properties.

On the contrary, artificial cores have advantages of flexible size, controllable properties, and convenient manufacture, many researchers have a favorable preference to artificial cores to conduct investigations (Xie, Lu, Li, Jiang, & Yu, 2016; Y. Zhao et al., 2017). Xie (Xie et al., 2016) adopted artificial sandstone composed of three layers cemented together to investigate the applicability of hydrophobically-associating-polymer (HAP) in the heterogeneous reservoir. Kong (Kong et al., 2019) employed a 3D positive rhythm artificial sandstone model to research foam block characteristics and transport mechanisms in the porous media. Permeability and wettability are quite often the most significant requirement for artificial cores as far as previous researchers are concerned, whereas in the conglomerate research pore structure is a fundamental parameter. However, previous artificial cores rarely concentrate on the issue of pore structure. According to Zhao (Y. Zhao et al., 2017) and Zheng(Zheng Mingming, 2016), pore-throat distribution of artificial core cemented by epoxy resin cemented performs narrow, which is significantly different from conglomerate. This issue is discussed in detail in section 2. Therefore, the research on controlling the pore structure of conglomerate is necessary and essential.

The objective of this paper is to introduce a method for controlling the pore structure of conglomerate in the artificial core. The structure is as follows. First, the problem and solution of pore structure in present artificial cores are discussed in detail in section 2. Then, a granularity-based method for controlling the pore-throat distribution of conglomerate was introduced in following section 3. Finally, the effect of granularity on permeability and pore-throat distribution is discussed in section 4.

2. Problem description and solution

According to the pore structure characterization of the current artificial core, it's difficult to control the complicated pore structure. For completeness and clarity, pore-throat distribution in the current artificial core is introduced in section 2.1. Then, the solution to the problem is described in section 2.2.

2.1 Current Situation of Pore Structure in artificial core

At present, most artificial cores were composed of quartz with different particle sizes and cemented by epoxy resin. Nevertheless, the epoxy resin would firmly stick to the surface of sand or gravel, which makes nano-scale pores completely sealed. That explains why nano-pore rarely exists in resin-based artificial cores. Figure 1 shows there exists rare nano-pore in the resin-based artificial core regardless

of permeability of 590mD or 81mD. Although most frequent pore-throat (the pore-throat radius corresponding to the maximum frequency) of the artificial core with a permeability of 590mD and 81mD are respectively 10μm and 4μm, the morphology of pore-throat distribution performs uniform, which is different from the bimodal or multimodal conglomerate. Therefore, if adopting a resin-based artificial core, complicate pore structure such as various fashion of pore-throat distribution could hardly be achieved. It is essential to explore a solution to complicate pore structure.

2.2 Solution to Complicate the Pore-Throat Distribution

In this work, Portland cement was selected to substitute for epoxy resin as cementation in the artificial core. Unlike epoxy resin, Portland cement is filled in the pores where the sand or gravel is packed. Moreover, a crosslinked reaction is performed in the pores during the cement solidification to form secondary minerals such as aluminum oxide, calcium sulfate, and calcium carbonate. The secondary minerals could cement rock grains, and its special lattice characterization and microcrack are conducive to the formation of nano-scale pores. Figure 2 demonstrates there exists wider pore-throat distribution in cement-bound artificial core. Especially the proportion of nano-pore performs significantly higher than the resin-based core. Therefore, the method that epoxy resin was substituted for Portland cement in the artificial core could provide an effective solution to make pore-throat distribution more complicated. Based on this method, various morphology and characterization of pore structure in artificial conglomerate could be achieved.

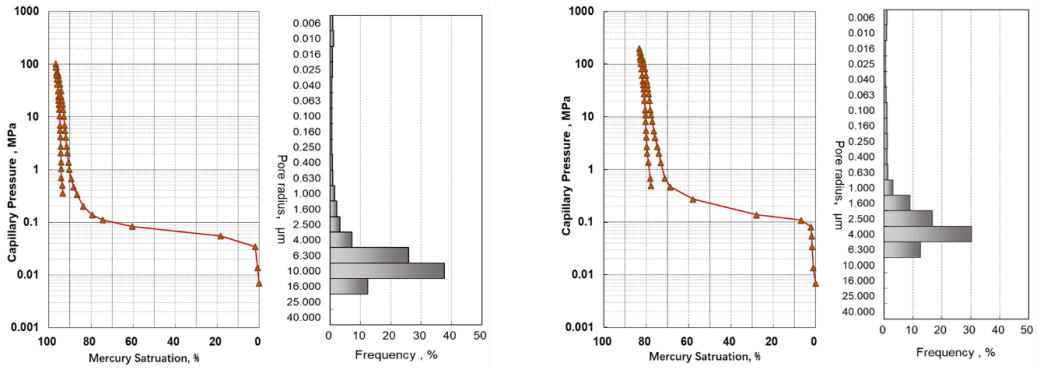

Figure 1 Capillary pressure and pore-throat distribution in artificial core cemented by epoxy resin. (a) artificial core with a permeability of 590mD. (b) artificial core with a permeability of 81mD.

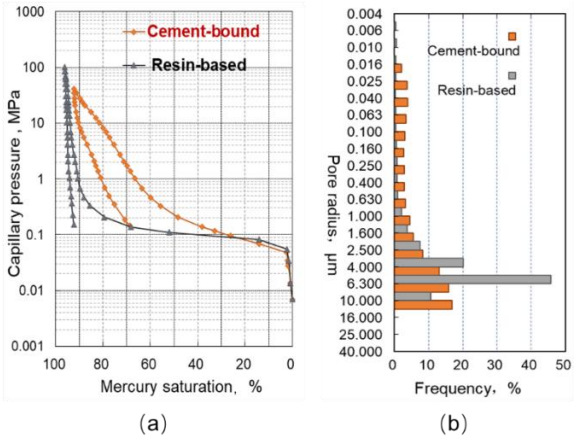

Figure 2 Capillary pressure and pore-throat distribution of resin-based and cement-bound artificial core with similar permeability of 230mD. The gray line is a resin-based artificial core. The orange line is a

cement-bound artificial core.

3. Methods for Controlling Pore Structure

We proposed a method for controlling the pore structure by changing the granularity of gravel or sand. Although there exist many parameters, such as average grain size, standard deviation, skewness, and kurtosis, presenting the granularity distribution of sedimentary rock, the interactive influence among these parameters makes it difficult to investigate the relationship between a single variable and pore distribution. Hence, we introduce a characterization method of granularity distribution in section 3.1. Then, the fabrication of artificial core is introduced in section 3.2. Finally, we provide a statistical approach to quantify the relationship between particle size and pore distribution in section 3.3, which could make it more effective to achieve control of the pore structure.

3.1 The Proposal of Bimodal Grain Size Curve

Normally conglomerate is composed of grains with various granularities. It is the combination of grains with various granularity that results in a special packed structure such as bimodal or multimodal. However, the granularity distribution of conglomerate was complicated and hard to describe. Hence how to describe the distribution characterization of granularity was the key to explore the relationship between particle size and pore structure.

In the aspect of representing method to grain size represent. Krumbein and Deoglas (Doeglas, 1946; Krumbein, 1938) speculated that the sedimentary granularity conformed to a multi-population mixed log-normal distribution. Visher (Visher, 1969) adopted a log-probability plot to separate three straight lines composed of suspension, saltation, and rolling, which was concerning the sedimentary process and sedimentary dynamics. Each straight line was referred to as a sub-population of the log-normal distribution. However, Ehrlich and Qu (Ehrlich, 1983; Qu, 1990) pointed out the number of straight lines presenting sub-population might not be equivalent to the sub-population of the log-normal distribution. To solve the problem, Qu (Qu, 1990) has indicated that the granularity of sedimentary was a mixture of two or three log-normal distribution.

Based on this understanding, we emphasized that the grain size of conglomerate is composed of two log-normal distribution. By regulating the two log-normal distribution parameters, various fashion grain size curves of the artificial core could be achieved.

The detailed formula of bimodal grain size distribution is as follow:

$$f(\Phi)=\frac{C}{\sqrt{2\pi}\sigma_1}\cdot\exp\left(-\frac{(\Phi-\mu_1)^2}{2\sigma_1^2}\right)+\frac{1-C}{\sqrt{2\pi}\sigma_2}\cdot\exp\left(-\frac{(\Phi-\mu_2)^2}{2\sigma_2^2}\right) \quad (1)$$

Where $f(\Phi)$ is grain density distribution, ranging from 0 to 1. Φ is granularity Φ, calculated by the formula $\Phi = -log_2 D$, where D is the maximum diameter of the particle (mm). The smaller the granularity Φ is, the larger the grain size performs. C is the relative weight, ranging from 0 to 1. μ_i is the average value of the i-th log-normal distribution, the value is equivalent to the granularity Φ corresponding to the maximum value of this log-normal distribution. σ_i is the variance of the i-th log-normal distribution, the larger the value is, the wider the log-normal distribution performs. Furthermore, we define the log-normal distribution with smaller granularity Φ as the coarse grain peak (CGP). Similarly, the log-normal distribution with larger granularity Φ was defined as the fine grain peak (FGP).

Aiming to verify the feasibility of this method, a total of 41 samples from Karamay oilfield, whose lithology consisted of conglomerate, sandy conglomerate, sand-bearing conglomerate, and sandstone, were selected to evaluate the accuracy of the bimodal grain size model.

The least-square method was employed to solve the fitting parameter, such as the relative weight C, average value, and variance of each log-normal distribution. The objective function is as follow:

$$\min_{x} \left\| F\left(C_i, \mu_i, \sigma_i, xdata\right) - ydata\left(xdata\right) \right\|^2 \tag{2}$$

$$F\left(x, xdata\right) = \sum_i C_i \cdot \int_{-\infty}^{+\infty} \frac{1}{\sqrt{2\pi}\sigma_i} e^{-\frac{(x-\mu_i)^2}{2\sigma_i^2}} dx \tag{3}$$

$$Constra\,\mathrm{int}: \sum_i C_i = 1, C_i \geq 0, \mu_1 > \mu_2 \tag{4}$$

The trimodal (i=3 in the formula(3)) and bimodal (i=2 in the formula(3)) grain size model were respectively evaluated via the above mention approach. As shown in Figure 3, all scatters were in the area above the baseline, indicating that the fitting effect of the trimodal grain size model generally performed better than that of the bimodal model. Although it has been proven that the greater the number of log-normal distributions in the mixed model, the higher the fitting accuracy performed, R-Square of the bimodal grain size model ranged from 0.96 to 0.98, which demonstrated that the bimodal model did accurately characterize the sedimentary grain-size curve. Therefore, it's actionable to regulate various fashion of grain size curve through the superimposed of two log-normal distribution.

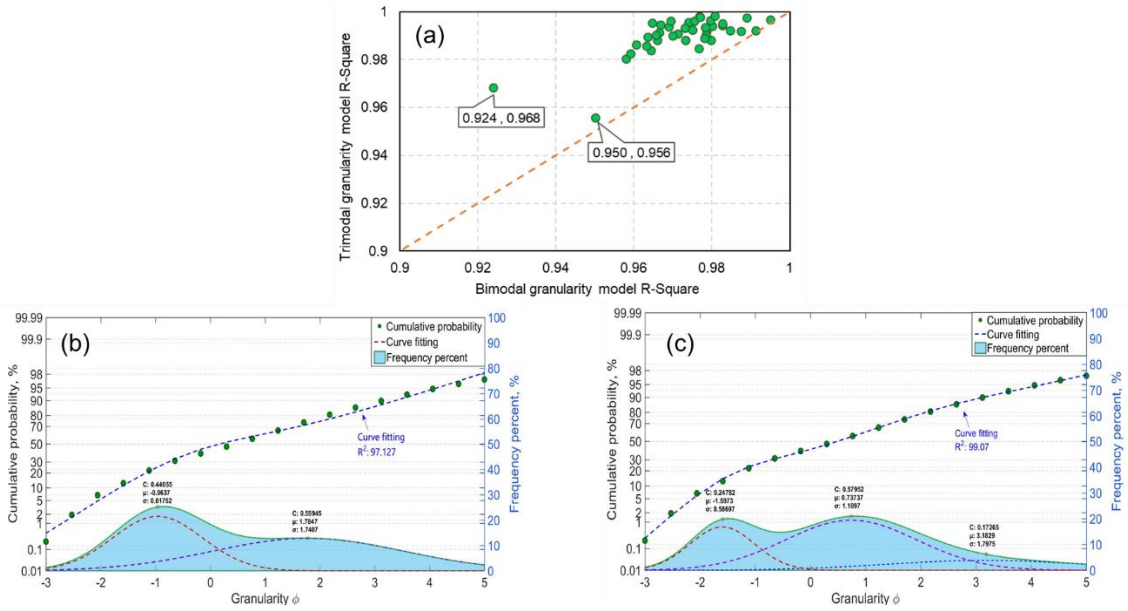

Figure 3 Contrast between the bimodal granularity model and the trimodal granularity model. (a) cross plot of bimodal granularity model R-Square versus trimodal model R-Square. The orange dashed line is the baseline, reflecting the condition that the R-Square of the bimodal model is equivalent to that of the trimodal model. (b) and (c) respectively represents curving fitting adopting bimodal and trimodal granularity modal. Scatters are cumulative probability corresponding to various granularity Φ. The Blue dashed line represents the prediction curve employing the multimodal granularity model. The Blue area represents the grain density distribution composed of multiple log-normal. The red and purple dashed line respectively represents coarse and fine log-normal distribution. The blue dotted line in the area represents the ultra-fine log-normal distribution.

3.2 The Fabrication Procedure of Artificial Core

3.2.1 Material

In theory, natural sandy gravel or fragments from cores should be selected as a grain of artificial core. However, the composition of natural gravel sediments is uncontrollable and varied, which makes it difficult to ensure high similarity among different batch of supplying materials. It brought a great deal of hardship on the parallelism of artificial cores. Hence, we gave preference to sand or gravel composed of a single mineral rather than natural gravel composed of the complicated mineral.

The material in detail consisted of quartz sand, potassium feldspar, plagioclase, river sand, and biotite, whose grain size ranged from 3 to 320 mesh. Sandy conglomerate is characterized by low maturity of mineral composition, indicating feldspar and debris account for a large proportion. In terms of materials, quartz sand and feldspar were respectively selected as quartz and feldspar components, then river sand and biotite were selected as the debris component. It should be noted that quartz sand was made through thermoluminescence of quartz mechanical crushing and possessed high purity of quartz. Unlike quartz sand, river sand was produced in the riverbed where gravels were scoured repeatedly and possessed complicate mineral compositions, such as debris from volcanic or metamorphic rocks. This was the reason that river sand was selected as the component of debris.

Cementing material consisted of a cementing agent, crosslinking agent, and curing agent. The cementing agent and curing agent were respectively Portland cement and salinity water. The crosslinking agent could be composed of ammonium phosphate and aluminum fluoride.

3.2.2 Fabrication procedure

Quartz sand, feldspar, and river sand with grain size ranging from 3 to 320 mesh were mixed together according to grain size distribution curve and then mixed with cementation fluid composed of Portland cement, crosslinking agent, and curing fluid. Screen mesh was used to filter out aggregated particles to ensure more homogeneous cementation. The mixture was placed into assembled mold and beard compaction pressure for approximately half an hour. Until the core in the modal was initially solidified, an additional curing agent was added to ensure the formation of secondary mineral and cementation. It's cured at ambient temperature for three to five days. Finally, artificial core with various shape was cut, such as columnar Φ38mm or rectangular core with a width and height of 45mm and length of 300mm.

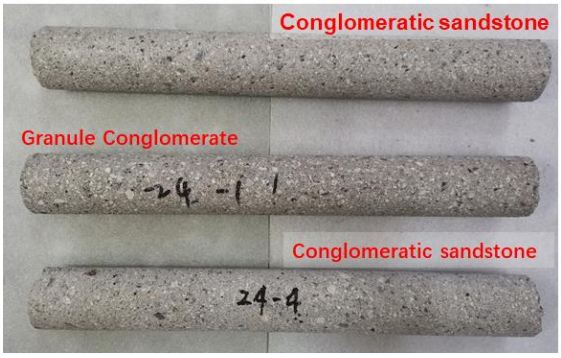

Figure 4 Artificial conglomerates with a size of Φ38×300mm made by experiments. The top and bottom are conglomeratic sandstone, while the middle is granule conglomerate.

3.3 The Statistical Approach to quantify the relationship between particle size and pore distribution

3.3.1 The Quantitative Characterization of Pore-Throat Distribution

The pore-throat distribution was measured by Mercury Injection Porosimeter (MIP). Although several parameters such as average pore-throat radius, sorting coefficient, kurtosis, and structural coefficient could characterize the pore structure of porous media, these are not sufficient to characterize distribution morphology and predict pore-throat distribution in more detail. In this work, similar to the grain size distribution characterization, the pore-throat distribution could be characterized as well by a bimodal model composed of two log-normal distribution.

The formula of pore-throat distribution is as follow:

$$f\left(\Phi^P\right)=\frac{C^P}{\sqrt{2\pi}\sigma_1^P}\cdot\exp\left(-\frac{\left(\Phi^P-\mu_1^P\right)^2}{2\left(\sigma_1^P\right)^2}\right)+\frac{1-C^P}{\sqrt{2\pi}\sigma_2^P}\cdot\exp\left(-\frac{\left(\Phi^P-\mu_2{}^P\right)^2}{2\left(\sigma_2^P\right)^2}\right) \tag{5}$$

Where $f\left(\Phi^P\right)$ is a function of pore-throat frequency distribution, ranging from 0 to 1. Φ^P is the granularity of pore-throat, calculated by the formula $\Phi^P=\text{-}log_2D^P$, where D^P is the pore-throat diameter (μm). C^P is the relative weight, ranging from 0 to 1. $\mu_1{}^P$ and $\sigma_1{}^P$ are average and variance of micro-scale pore-throat distribution. $\mu_2{}^P$ and $\sigma_2{}^P$ are respectively average and variance of the nano-scale pore-throat distribution. We define the log-normal distribution with pore-throat granularity less than zero as a micro-scale pore peak (MSPP) and pore-throat granularity great than zero as nano-scale pore peak (NSPP).

Furthermore, aiming to describe the pore-throat distribution morphology in more detail, the ratio of the maximum frequency of MSPP to that of NSPP was defined as the distribution morphology coefficient (DMC). The detailed formula is as follow:

$$DMC=\frac{C^P\cdot\sigma_2^P}{\left(1-C^P\right)\cdot\sigma_1^P} \tag{6}$$

The larger DMC performs micro-scale pore account for a larger proportion, in which the pore-throat distribution morphology is closer to a single log-normal distribution.

3.3.2 Genetic Programming procedure

Although the influence factors of pore structure could be qualitatively investigated via single-factor analysis, the pore structure is actually influenced by multiple factors. It's these important factors that lead to a dramatic increase in experiment design. Whether checkboard design requires considerable schemes or orthogonal experimental design that is controversial in the quantification could hard quantify the relationship between grain size distribution and pore-throat distribution. Furthermore, Genetic Programming (GP) could effectively solve this problem. It is the reason that Genetic programming was employed in this work.

GP adopted a tree representation method to realize the evolution of mathematical functions, operators, and even conditional statements(Sette & Boullart, 2001). Similar to the Genetic Algorithm (GA), evolution is achieved by crossover, mutation, and direct reproduction operators. Crossover and mutation respectively exchange the sub-trees from the parents to reproduce the children and substitute

a random sub-tree of one parent with next-generation(Bahrami, Kazemi, Mahdavi, & Ghobadi, 2016). An example is shown in Figure 5. The direct reproduction operator is that offspring perform the same as one parent. Through each generation with evolution, the best solution could be obtained in terms of coefficient of determination (R^2). The R^2 are presented in Eqs(6).

$$R^2 = 1 - \frac{\sqrt{\sum_i \left(y_{pre,i} - y_{\exp,i}\right)^2}}{\sqrt{\sum_i y_{\exp,i}^2}} \tag{7}$$

Where y_{pre} is the prediction value through the GP model. y_{exp} is the actual test result.

In this work, a total of 56 samples of artificial sandy conglomerate were fabricated and evaluated through the GP method. The input variable included grain size distribution parameters, such as average value and variation of CGP and FGP, and cement content. Different pore structure features, for instance, average pore-throat radius, distribution morphology, and sorting coefficient could be respectively quantitatively evaluated.

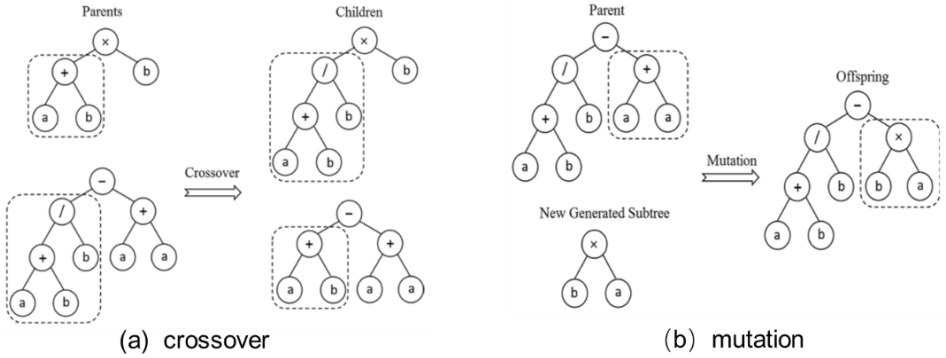

Figure 5 The schematic diagram of crossover and mutation operator. Cited by Bahrami et al., 2016

4. Results and Discussion

In the following, the influence of CGP and FGP on pore-throat distribution are respectively demonstrated in section 4.1. Pore-throat distribution and grain size respectively affect the permeability and lithology of the artificial core. Hence, how permeability and lithology was affected by grain size are analyzed in section 4.2 and 4.3. Last of all, the relationship between pore-throat distribution morphology and lithology or permeability is quantitatively analyzed in section 4.4.

4.1 Effect of Particle Size Distribution on Pore Distribution

4.1.1 Effect of Fine Grain Peak (FGP) on Pore Distribution

The artificial cores with FGP average value μ_2 of 1.25, 2.25, and 3.75 at the same CGP granularity Φ of -0.75 were fabricated. The distribution of grain size and pore-throat are shown in Figure 6 and Table 1. As FGP average value μ_2 changes from large to small, which means the grain size of mineral performs coarser, the grain size morphology gradually changes from bimodal to unimodal, and the average pore-throat radius increases from 1.2μm to 5.57μm, while the most frequent pore-throat radius increases from 1.0μm to 10μm, the frequency of pore ranging from 8 to 16μm perform more and more.

As for the morphology of the capillary pressure curve, with the decrease of FGP average value μ_2, the curve with capillary pressure lower than 1MPa gradually changes from convex to concave. Similarly, the relative sorting coefficient (represents the variation coefficient of pore-throat) becomes

lower, which indicates that the sorting of pore gradually performs better.

It could be explained that plenty of matrices make the large pores among pebbles be widely filled, then large pores over 10μm is substituted for small pore less than 5μm. Meanwhile, the difficulty in driving pore-throat obviously increases. It could be proven that displacement pressure performs larger with smaller average value μ_2 of FGP (Table 1).

It could be noted that cavities could be formed among gravels with grain size over 2cm, in which matrix filled might be mud, silt, medium sand, and even coarse sand. As depicted in Figure 6, silt sand with granularity Φ ranging from 3 to 5 could result in a larger proportion of pores ranging from 0.4 to 1.6μm. Similarly, the medium-fine sand with granularity Φ ranging from 1.5 to 3 is conceived to form the pore ranging from 1.6 to 6.4μm, the coarse-medium sand with granularity Φ ranging from 0.5 to 1.5 is conceived to a larger proportion of pore ranging from 6.4 to 16μm.

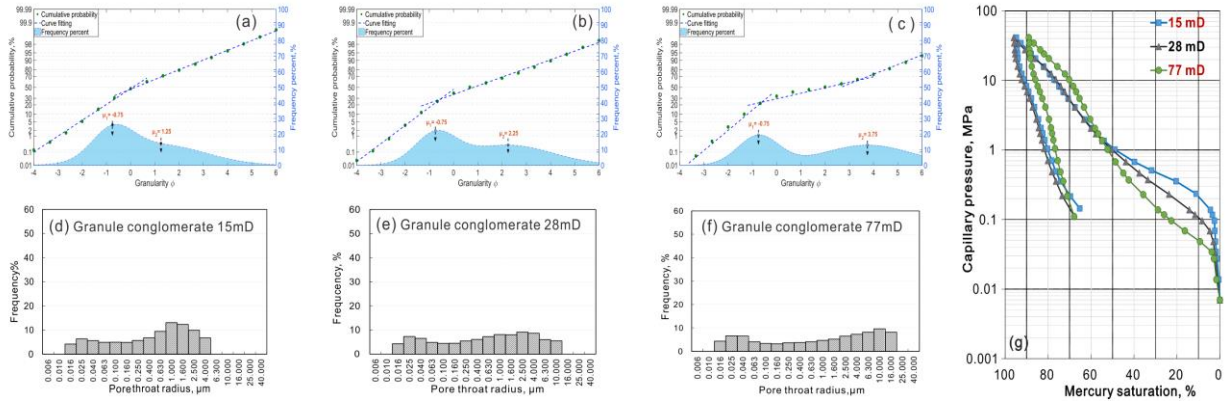

Figure 6 Capillary pressure curve and distribution of grain size and pore-throat in artificial conglomerate with various FGP average value μ_2. (a)-(c) respectively represent grain size distribution with FGP average value μ_2 of 3.75, 2.25, and 1.25. (d)-(f) respectively represent pore-throat distribution with various μ_2 value. (g) capillary pressure curve of artificial conglomerate with various μ_2 value.

Table 1

Pore structure characteristics of artificial cores with various lithology and permeability

Lithology	Value of μ_1	Value of μ_2	Permeability (mD)	Porosity (%)	Pore-throat radius (μm)		Relative sorting coefficient	Displacement pressure(MPa)
					Average	Most frequent		
Granule conglomerate	-0.75	3.75	15	19.04	1.242	1.0	2.724	0.138
		2.25	28	17.69	2.811	2.5	1.588	0.048
		1.25	77	18.78	5.573	10	0.998	0.034
Granule conglomerate	-0.75	2	48	19.22	3.592	6.3	2.043	0.068
Conglomeratic coarse sandstone	0.5		81	14.25	4.371	4.0	0.873	0.048
Medium sandstone	1.8		109	18.58	5.149	4.0	0.706	0.048

4.1.2 Effect of Coarse Grain Peak (CGP) on Pore Distribution

Similarly, the artificial cores with various CGP average value μ_1 at the same FGP average value μ_2 of 2 were fabricated. The distribution of grain size and pore-throat are shown in Figure 7 and Table 1. As shown in Figure 7, the CGP average value μ_1 changes from small to large, which means that CGP moves from left to right in the horizontal coordinate of granularity Φ, the lithology successively transform into granule conglomerate, conglomeratic coarse sandstone, and medium sandstone, and the curve morphology gradually changes from bimodal to unimodal. The curve morphology of capillary pressure less than 1MPa gradually transforms from straight to concave, which indicates that pore-throat

sorting performs better, as proven by the reduction of the relative sorting coefficient. In summary, whether the offset of CGP or FGP, sorting characteristics of grain size predominantly determine the sort characteristics of pore-throat.

Different from the effect of FGP on pore-throat distribution, the smaller gap between CGP and FGP and smaller average grain size make most frequent pore-throat radius decrease from 6.3μm of granule conglomerate to 4.0μm of medium sandstone. However, the average pore-throat radius increases from 3.59μm of granule conglomerate to 5.15μm of medium sandstone (Table 1).

Without secondary filling in the pores, there exists a favorable positive correlation between the pore-throat radius and grain size. In granule conglomerate, coarse sand and fine-gravel stacked on the top of each other are conceived to form plenty of pore over 6μm. Meanwhile, the proportion of matrix filled in these pores is limited, which results in that a large number of pores over 6μm could be preserved. It explains the reason that most frequent pore-throat radius of granule conglomerate perform larger than that of conglomeratic coarse sandstone and medium sandstone.

In addition, when the grain distribution morphology gradually transforms into unimodal, the medium sand, which accounts for a large proportion, result in a large proportion of pore-throat ranging from 2 to 6μm. It explains the reason that the average pore-throat radius of medium sandstone performs larger than that of granule conglomerate, even though most frequent pore-throat radius of medium sandstone performs smaller than that of granule conglomerate.

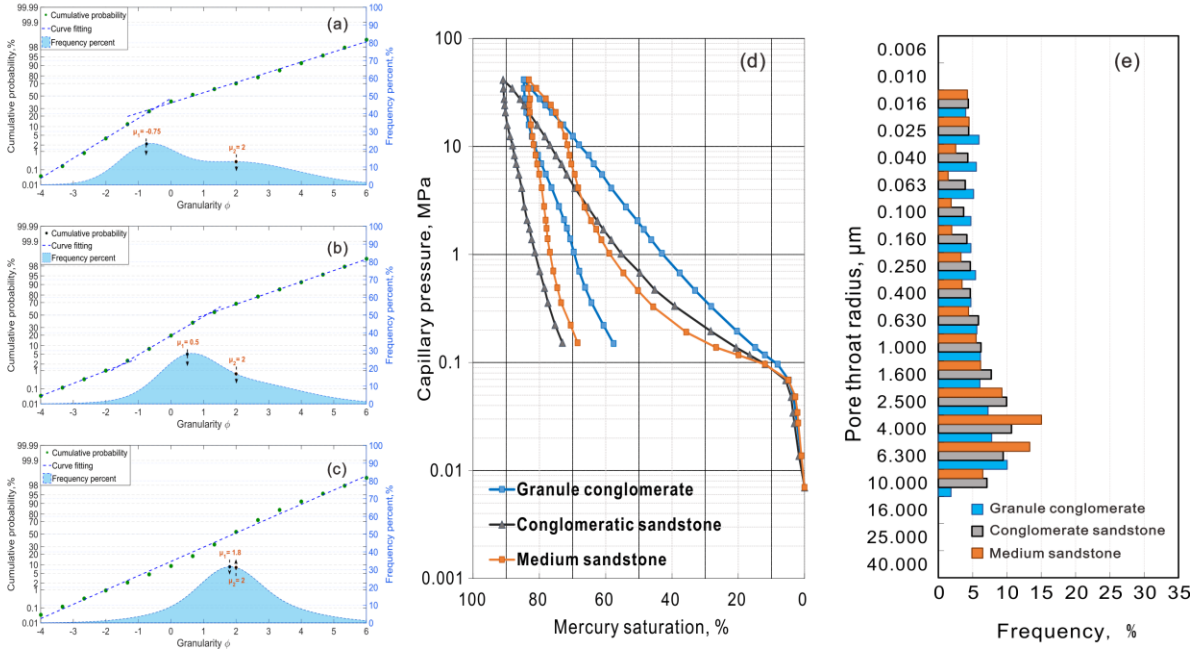

Figure 7 Capillary pressure and distribution of grain size and pore-throat. (a)-(c) represent the grain size distribution with CGP average value μ_1 of -0.75, 0.5, and 1.8. (d) capillary pressure curve with various CGP average value μ_1. (e) pore-throat distribution with various CGP average value μ_1.

4.1.3 The Quantitative Relationship between Average Pore-Throat Radius and Particle Size

A total of 42 artificial cores with various grain size distribution were fabricated, the pore structure of which was tested by Mercury Injection Porosimetry (MIP). The relationships between grain size characterization and average pore-throat radius were investigated through the GP algorithm. The average pore-throat radius satisfies the following:

$$R_P = 28.75 - 5.64 \cdot \bar{\sigma} + (0.005 \cdot M_m - 9.50) \cdot \mu_v - (0.005 \cdot M_m + 1.87) \cdot \bar{\mu} - 0.005 \cdot M_m \cdot \sigma_v \quad (8)$$

Where $\bar{\mu}$ is the average grain size, which is calculated by $\bar{\mu} = C\mu_1 + (1-C)\mu_2$. μ_v is the variation coefficient of average values of bimodal grains, which is calculated from equation $\mu_v = \frac{\sqrt{C(\mu_1 - \bar{\mu})^2 + (1-C)(\mu_2 - \bar{\mu})^2}}{\bar{\mu}}$, M_m is the grain size of the finest sand, mesh, the value normally ranges from 200 to 500. $\bar{\sigma}$ is the average variation of grain size, which is calculated by $\bar{\sigma} = \frac{\sigma_1 \sigma_2}{C\sigma_2 + (1-C)\sigma_1}$. σ_v is the variation coefficient of variation of bimodal grains, which is calculated by $\sigma_v = \frac{\sqrt{C(\sigma_1 - \bar{\sigma})^2 + (1-C)(\sigma_2 - \bar{\sigma})^2}}{\bar{\sigma}}$.

As shown in Eq.(8), the larger difference between double grain peaks, such as average values and variation, and the smaller average grain size might result in a decrease in the average pore-throat radius. Figure 8 shows the comparison between calculations via Eq.(8) and measured data of the average pore-throat radius. It is feasible to control the average pore-throat radius of artificial cores through the aforementioned formula.

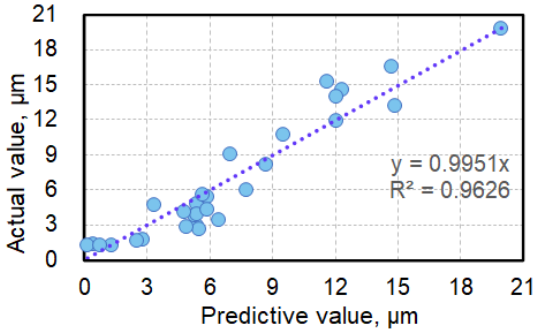

Figure 8 Comparison of calculations through Eq.(8) with measured data of average pore-throat radius. The blue dash curve presents the condition that prediction is equivalent to experimental data.

4.2 Effect of the offset of Grain Peaks on Permeability

In terms of permeability, the relationship between grain size distribution and permeability is discussed in this section. Hence, artificial cores with various grain size were fabricated, the grain size distribution of artificial cores was designed from two perspectives: On one hand, various FGP average value μ_2 change at the same CGP average value μ_1. On the other hand, CGP average values μ_1 change while FGP average values μ_2 remain constant.

As shown in Figure 9(a), as the FGP average value μ_2 increases from 0.25 to 3, which means the fine grain size perform smaller and smaller, the permeability decreases significantly from 2000mD to 16mD with the different trend. Permeability of granule conglomerates decreases in a trend of powder law with the decrease of fine grain size. In contrast, the permeability of conglomeratic coarse sand and sandstone decreased exponentially.

The phenomenon that the decreasing trend of permeability varies by lithology could be explained by various stacking structures of grains. As the proportion of granule in the conglomerate performs greater than 50%, there exists plenty of pores over 10μm. As FGP average value μ_2 increases, which means more proportion of medium-fine sand and even mud, the large pores are generally filled in

multiscale packing structure, i.e., the gravel-grade pore spaces are filled with sand and sand-grade pore spaces are filled with mud, the multiscale packing structure results in a faster decreasing rate of permeability in the conglomerate than sandstone. On the other hand, due to the dominated proportion of sands in conglomeratic coarse sandstone and sandstone, the pore-throat radius among the sand-grade grains account performed obviously smaller than that among gravel-grade grains. Thus it is difficult to form the multiscale packing structure. It explains the similar decreasing trend in conglomeratic coarse sandstone and sandstone.

As shown in Figure 9(b), as the CGP average value μ_1 increases from to -1.75 to 1.8 at the same FGP average value μ_2 of 2, the lithology successively transforms into sandy-conglomerate, granule conglomerate, conglomeratic coarse sandstone, coarse sandstone, and medium sandstone. Meanwhile, the distance between CGP and FGP becomes smaller, in which grain size distribution morphology transforms from bimodal to unimodal, permeability increases from 27mD, and then gradually stabilizes at approximately 110mD. In summary, the sorting of grain has an obviously positive correlation with permeability.

The phenomenon could be explained by a special packing structure. In the granule conglomerate or sandy conglomerate, large pore spaces among gravel-grade grains are easily filled by sand-grade and mud-grade matrix. As aforementioned, a multiscale packing structure named as the multimodal structure is formed. It's this special structure that results in that permeability of conglomerate performs lower than that of sandstone in the condition of similar matrix content. For another, as the sorting of grain size performs better, complicated packing structure is hard to form in well-sorted sand-grade grains, which results in that the main pore-throat radius performs larger. It explains the reason that grain sorting has a positive correlation with permeability.

In summary, whether in artificial sandstone or conglomerate, control of permeability is achieved by adjusting the FGP average value μ_2.

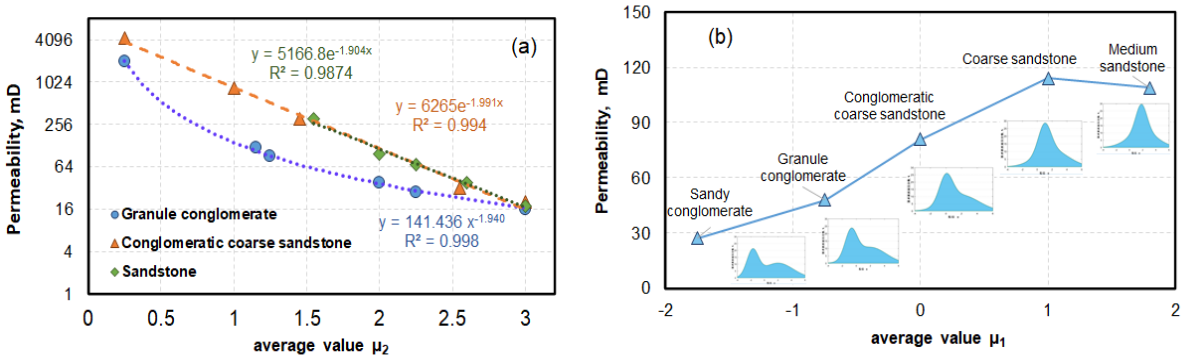

Figure 9 Permeability versus average value μ_1 and μ_2. (a) the blue circle scatters represent granule conglomerate with CGP average value μ_1 of -0.75. The orange triangle scatters represent conglomeratic coarse sandstone with CGP average value μ_1 of 0. The green square scatters represent sandstone with CGP average value μ_1 of 1.5. (b) the blue area graphs represent grain size distributions of various CGP average values at the same FGP average value μ_2 of 2.

4.3 Effect of the offset of Grain Peaks on Lithology

It's widely known that grain size curves are closely correlated with lithology. According to the relative proportion of pebble, granule, coarse sand, medium sand, fine sand, and silt sand (Table 2), the lithology is divided into five categories, including pebble conglomerate, granule conglomerate, sandy conglomerate, conglomeratic sandstone, coarse to fine sandstone.

We selected the grain size characteristics of nature core samples from Karamay oilfield in this work. Grain size distributions with various average values μ_1 and μ_2 were analyzed and named according to the aforementioned classification.

As shown in Figure 10(c), the marker point moves from a_1 to a_2, which reflects that FGP average value μ_2 performs larger, and the grain size of FGP performs smaller, the lithology is invariable granule conglomerate. In contrast, the point moves from a_2 to a_3, which reflects that the grain size of CGP performs smaller in the condition of similar matrix content, the lithology transform from granule conglomerate to conglomeratic sandstone.

In summary, even though FGP average value μ_2 could affect the lithology to some extent, CGP average value μ_1 is a dominant factor in the control of lithology. Generally, lithology is mainly determined by the proportion and size of coarse grain. Fine grains exert a limited influence on lithology. Therefore, various lithology of the artificial core could be achieved by adjusting CGP average value μ_1.

Table 2

Granularity Φ and grain sizes corresponding to the various grade of grains

Grain type	Gravel		Sand			
Grain grade	Pebble	Granule	Coarse sand	Medium sand	Fine sand	Silt sand
Grain size (mm)	4 ~ 64	2 ~ 4	0.5 ~ 2	0.25 ~ 0.5	0.1 ~ 0.25	0.01 ~ 0.1
Granularity Φ	-6 ~ -2	-2 ~ -1	-1 ~ 1	1 ~ 2	2~3.32	3.32 ~ 6.64

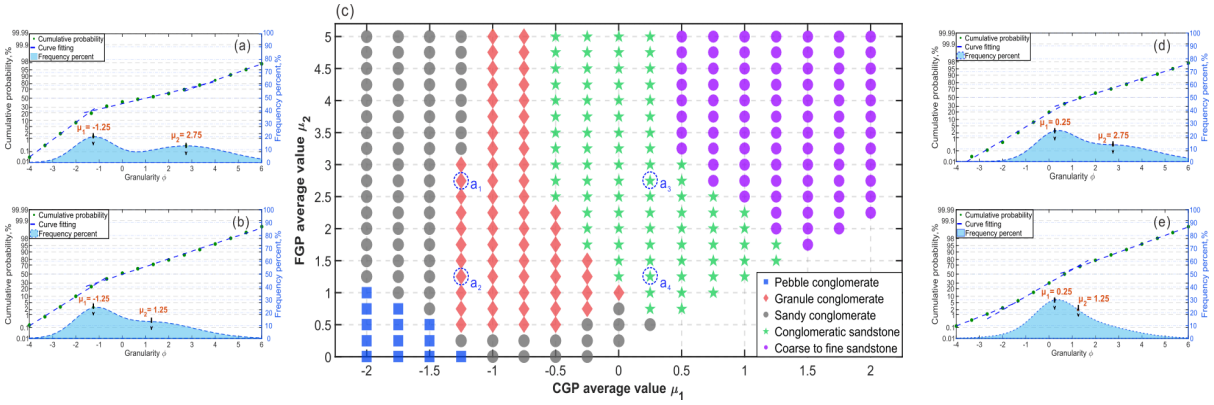

Figure 10 Cross plot of lithology corresponding to various CGP average value μ_1 and FGP average value μ_2. (a)(b)(d)(e) represent the grain size distribution at point a_1, a_2, a_3 and a_4 in (c), respectively. (a)(b) and(d)(e) reflect the offset process of FGP. (a)(d) and (b)(e) reflect the offset process of CGP. It should be noted that the cross plot is plotted in the given condition of weight C of 0.4, CGP variation σ_1 of 0.85, and FGP variation σ_2 of 1.85.

4.4 Quantitative Control on Pore Distribution Morphology

A total of 52 pore-throat distribution of artificial cores were investigated. Distribution morphology was categorized into three types, including steep peak, hills, and plain. It's statistically reckoned that pore-throat distribution morphology performs "type of steep peak" for DMC great than 3.5, "type of hills" with DMC ranging from 2 to 3.5, and "type of plain" with DMC less than 2 (Figure 11).

Moreover, the relationship between the aforementioned features and DMC were quantitatively investigated through the GP algorithm. The result depicts as follow:

$$DMC = \frac{\overline{\sigma}}{\overline{\mu}} \cdot \left(\frac{269.8}{C_m} - 16.26 \right) + 2.33 \tag{9}$$

Where C_m is cement content, %. Normally, cement content satisfies the following empirical formula:

$$C_m = 0.232X_1 + 0.210X_2 + 0.176X_3 + 0.150X_4 + 0.126X_5 + 0.118X_6 \quad (10)$$

Where $X_1 - X_6$ are respectively the proportion of pebble, granule, coarse sand, medium sand, fine sand, and silt sand, %.

As shown in Eq.(9), pore-throat distribution morphology is determined by cement content and average grain size. Considering that average grain size generally performs more than zeros, there exists a critical point at cement content of 16.6%. While cement content performs more than 16.6%, the morphology of steep peek could hardly happen.

According to Eq.(9) and boundaries by DMC, the cross plot between pore-throat distribution morphology and lithology was derived (Figure 12). As shown in Figure 12, even for the same lithology, there exists various pore-throat distribution morphology, particularly in the conglomerate. The morphology of steep peaks exists in two regions, respectively in the well-sort conglomerate and in the sandstone. As aforementioned, well-sorted grain distribution results in the well-sorted pore-throat distribution. The pore space among pebble-grade grain is filled by coarse-to-medium sand to some extent, and the large pores over 10μm could be preserved due to insufficient fine-to-silt sand to fill these pores. It explains why the pore-throat distribution morphology performs a steep peak. As the proportion of fine-to-silt sand increases in the conglomerate, the multiscale accumulation in the grains inevitably happens, which results in complicated morphology such as hills or plains.

In the perspective of lithology, distribution morphology in most of granule conglomerates performs hills or plains, while that of in few well-sorted granule conglomerates performs steep peak. Sandy conglomerate is similar to the granule conglomerate. As lithology transforms from conglomerate to sandstone, the proportion of morphology of steep peaks performs larger. In the conglomeratic sandstone, the morphology of steep peak accounts for approximately 50%. The distribution morphology in conglomeratic sandstone is determined by gravel size and proportion. The larger the gravel size or proportion performs, the higher probability of morphology of hills performs. Last of all, the morphology of sandstone performs almost exclusively steep peaks.

The discussion that the morphology of pore-throat distribution varies by lithology was mentioned by Yin and Zhang (Yin Senlin, 2019; K. Zhang et al., 2020). The researchers also indicated that even for the same lithology such as granule conglomerate, the pore-throat distribution morphology perform various, which is attributed to the different accumulation structure corresponding to the various sedimentary environment. Hence, pore structure was analyzed according to the lithofacies or sedimentary environment. In this work, with the aid of artificial conglomerate fabrication, pore-throat distribution morphology is investigated from the perspective of grain distribution. Even though the relationship between lithology and morphology has been plotted in Figure 12, the boundaries of various morphology might not be very accurate. The trend should be correct because the multiscale packing structure occurs as the grain distribution transforms from unimodal to bimodal.

However, it should be noted that there exist applicable conditions in the cross plot of Figure 12. First of all, samples in Figure 12 are suitable in the condition of limited diagenesis, such as moderate compaction or cementation. Normally, the depth of actual reservoir should be less than 2000m. With the increase of compaction pressure or cementation, diagenesis performs more and more obvious. Even for the same grain distribution, it is diagenesis that decreases the proportion of large pores over 10μm

and makes the morphology of steep peak transform into that of hills or plain(Xiao, Wu, Yuan, Cao, & Xie, 2020; K. Zhang et al., 2020). Last of all, the cross plot was plotted in the specific parameter of grain distribution, which represents the alluvial fan of Karamay conglomerate reservoir. If another sedimentary environment was selected, for instance, a meandering river or delta deposit, the figure is no longer applicable. In summary, Figure 12 supports an ideal relationship between lithology and related morphology of pore-throat distribution within a specific alluvial fan.

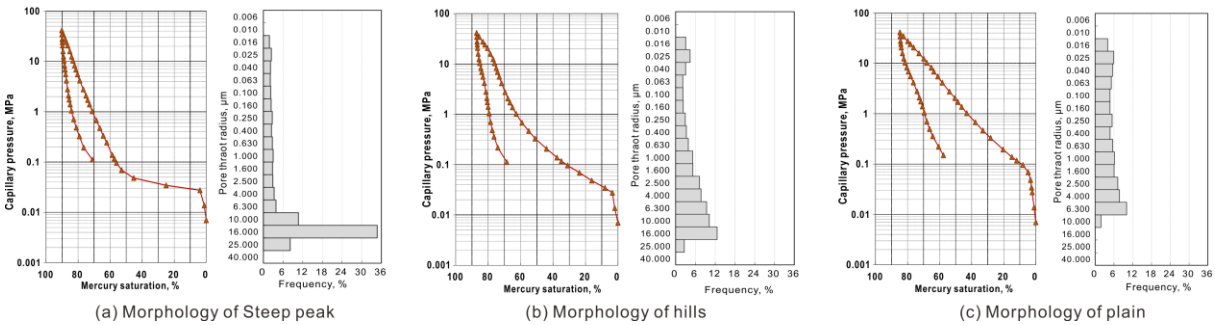

Figure 11 Various morphology of pore-throat distribution. (a) represents morphology type of steep peak, pore-throat distribution is closer to a single log-normal distribution. (b) presents the morphology type of hills, pore-throat distribution performs a combination of two peaks. (c) presents morphology type of plain, pore-throat distribution is analogous to flatland.

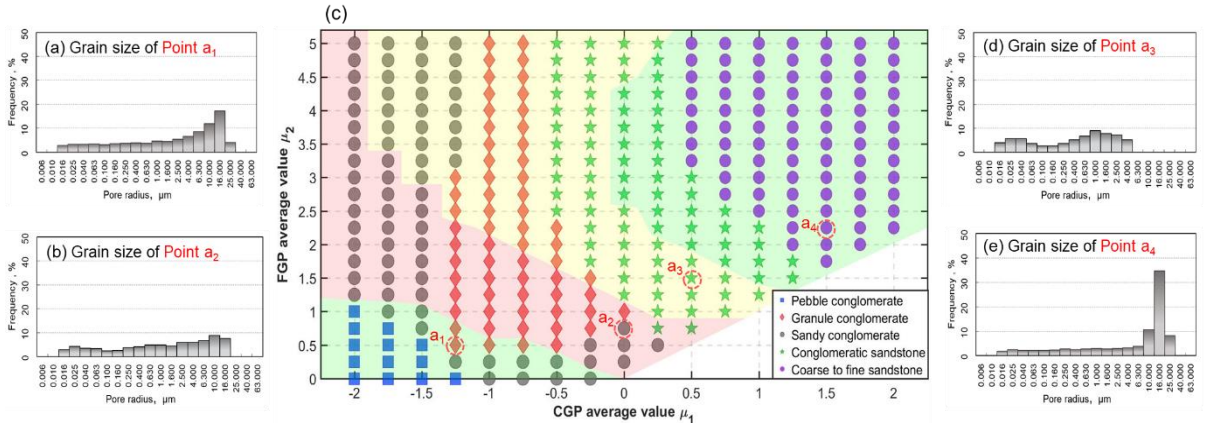

Figure 12 The relationship between pore-throat distribution morphology and lithology. (a)(b)(d)(e) are the pore-throat distribution of artificial cores with grain size distribution corresponding to the point a_1, a_2, a_3, and a_4 of (c), respectively. (c) the cross plot between distribution morphology and lithology. The green area represents the pore-throat distribution morphology of a steep peak. The yellow area represents the distribution morphology of hills. The red area represents the distribution morphology of the plain.

5. Conclusion

(1) Artificial conglomerates or sandstones with wider pore-throat distribution and more proportion of nano-scale pore space were developed, which overcomes the difficulty of centralized pore-throat distribution in epoxy-resin-based artificial cores. It's attributed to the phenomenon that Portland cement adopted as the main cementing agent could motivate the secondary reaction and simulate accurately mineral cementation and secondary changes.

(2) The bimodal grain size distribution model was proposed to design various morphology of grain size distribution. The curve of grain size distribution is composed of coarse grain peak (CGP) and fine grain peak (FGP). The various morphology of grain size distribution could be achieved by varying the

width, height, and granularity of CGP and FGP. Similarly, the pore structure in artificial cores could be controlled by designing different grain distribution.

(3) Lithology is mainly determined by the average value μ_1 of CGP. Similarly, the permeability of artificial cores is mainly determined by the average value μ_2 of CGP. There exists a positive correlation between permeability and sorting of grain, which means the better sorting of grain performs, the higher permeability is.

(4) With the offset of FGP from coarse to fine, most frequent and average radius of pore-throat decreases, the morphology of capillary pressure gradually transforms from convex to concave, and the sorting of pore gradually perform worse. Moreover, the accumulation of silt sand is conducive to pores with a radius ranging from 0.4 to 1.6μm, that of medium-to-fine sand is conducive to pores with a radius ranging from 1.6 to 6.4μm, while that of coarse sand contributes to pores with a radius ranging from 6.4 to 16μm.

(5) Considering that there exists multi morphology of pore-throat distribution in the conglomerate, morphology is categorized into three types, including steep peak, hills, and plain. Even for the same lithology, such as granule conglomerate or conglomeratic sandstone, there might exist two or even three morphology types of pore-throat distribution. The results demonstrate that pore-throat distribution morphology is mainly determined by grain diversity. As the distance or gap between CGP and FGP perform larger, which multiscale grain packing structure might occur, the morphology of pore-throat distribution transforms from steep peak to hills in the conglomerate. In contrast with the conglomerate, morphology in sandstone generally performs a steep peak because multiscale packing structure could hardly occur.

Acknowledgments

The work was supported by the National Natural Science Foundation of China (52074318). The authors express their appreciation to technical reviewers for their constructive comments. The data archiving is underway, a copy of data was uploaded as supporting information.

References

Bahrami, P., Kazemi, P., Mahdavi, S., & Ghobadi, H. (2016). A novel approach for modeling and optimization of surfactant/polymer flooding based on Genetic Programming evolutionary algorithm. *Fuel, 179*, 289-298. doi:https://doi.org/10.1016/j.fuel.2016.03.095

Clarke, R. H. (1979). Reservoir Properties of Conglomerates and Conglomeratic Sandstones. *AAPG Bulletin, 63*(5), 799-803.

Doeglas, D. J. (1946). Interpretation of the Results of Mechanical Analyses. In *SEPM Journal of Sedimentary Research* (Vol. 16).

Ebaga-Ololo, J., & Chon, B. H. (2018). Experimental investigation of the influence of salinity gradient on low-concentration surfactant flooding in Berea sandstone. *Journal of Industrial and Engineering Chemistry, 68*, 355-363. doi:https://doi.org/10.1016/j.jiec.2018.08.007

Ehrlich, R. (1983). Size analysis wears no clothes, or have movements come and gone? *Journal of Sedimentary Research, 53*, 1. doi:10.2110/jsr.53.1

Feng, C., Li, T., He, W., & Zheng, M. (2020). Organic geochemical traits and paleo-depositional conditions of source rocks from the Carboniferous to Permian sediments of the northern Mahu Sag, Junggar Basin, China. *Journal of Petroleum Science and Engineering, 191*, 107117. doi:https://doi.org/10.1016/j.petrol.2020.107117

Gao, M., Lv, J., Gao, J., Zhang, S., Wang, Q., Wang, X., & Chen, L. (2018). *The Characteristics and Adjustment Technology of Surfactant/Polymer Binary Flooding in Conglomerate Reservoir*. Paper presented at the SPE Kingdom of Saudi Arabia Annual Technical Symposium and Exhibition, Dammam, Saudi Arabia. https://doi.org/10.2118/192444-MS

Han, H., Li, S., Ma, D., Ji, Z., Yu, H., & Chen, X. (2018). Investigation of flue gas displacement and storage after the water flooding in a full diameter conglomerate long-core. *Petroleum Exploration and Development, 45*(5), 903-909. doi:https://doi.org/10.1016/S1876-3804(18)30093-4

Jin, L., Guiwen, W., Ziyuan, W., Jing, C., Xiaojiao, P., Shuchen, W., . . . Xuqiang, F. (2017). A review on pore structure characterization in tight sandstones. *Earth-Science Reviews*. doi:10.1016/j.earscirev.2017.12.003

Kang, X., Hu, W., Cao, J., Wu, H., Xiang, B., & Wang, J. (2019). Controls on reservoir quality in fan-deltaic conglomerates: Insight from the Lower Triassic Baikouquan Formation, Junggar Basin, China. *Marine and Petroleum Geology, 103*, 55-75. doi:https://doi.org/10.1016/j.marpetgeo.2019.02.004

Kareem, R., Cubillas, P., Gluyas, J., Bowen, L., Hillier, S., & Greenwell, H. C. (2017). Multi-technique approach to the petrophysical characterization of Berea sandstone core plugs (Cleveland Quarries, USA). *Journal of Petroleum Science and Engineering, 149*, 436-455. doi:https://doi.org/10.1016/j.petrol.2016.09.029

Kong, D., Li, Y., Yu, M., Ma, R., Guo, H., Peng, Y., . . . Yan, H. (2019). Experimental investigation on block and transport characteristics of foam in porous media for enhanced oil recovery processes. *Colloids and Surfaces A: Physicochemical and Engineering Aspects, 570*, 22-31. doi:https://doi.org/10.1016/j.colsurfa.2019.02.067

Krumbein, W. C. (1938). Size Frequency Distributions of Sediments and the Normal Phi Curve. *Journal of Sedimentary Research, 8*(3), 84-90.

Lin, Q., Bijeljic, B., Pini, R., Blunt, M. J., & Krevor, S. (2018). Imaging and Measurement of Pore-Scale Interfacial Curvature to Determine Capillary Pressure Simultaneously With Relative Permeability. *Water Resources Research, 54*(9), 7046-7060. doi:10.1029/2018wr023214

Liu, Z., Li, Y., Leng, R., Liu, Z., Chen, X., & Hejazi, H. (2020). Effects of pore structure on surfactant/polymer flooding-based enhanced oil recovery in conglomerate reservoirs. *Petroleum Exploration and Development, 47*(1), 134-145. doi:https://doi.org/10.1016/S1876-3804(20)60012-X

Liu, Z., Li, Y., Lv, J., Li, B., & Chen, Y. (2017). Optimization of polymer flooding design in conglomerate reservoirs. *Journal of Petroleum Science and Engineering, 152*, 267-274. doi:https://doi.org/10.1016/j.petrol.2017.03.010

Ma, Y., Hou, J., Zhao, F., & Song, Z. (2018). Linearly descending viscosity for alkaline-surfactant-polymer flooding mobility modification in multilayer heterogeneous reservoirs. *Rsc Advances, 8*(15), 8269-8284. doi:10.1039/c8ra00362a

Mahmic, O., Dypvik, H., & Hammer, E. (2018). Diagenetic influence on reservoir quality evolution, examples from Triassic conglomerates/arenites in the Edvard Grieg field, Norwegian North Sea. *Marine and Petroleum Geology, 93*, 247-271. doi:https://doi.org/10.1016/j.marpetgeo.2018.03.006

Markussen, Ø., Dypvik, H., Hammer, E., Long, H., & Hammer, Ø. (2019). 3D characterization of porosity and authigenic cementation in Triassic conglomerates/arenites in the Edvard Grieg field using 3D micro-CT imaging. *Marine and Petroleum Geology, 99*, 265-281. doi:https://doi.org/10.1016/j.marpetgeo.2018.10.015

Migoń, P. (2020). Geomorphology of conglomerate terrains – Global overview. *Earth-Science Reviews, 208*, 103302. doi:https://doi.org/10.1016/j.earscirev.2020.103302

Qiang, L., Liehui, Z., Hongming, T., Yulong, Z., Man, C., & Chunyu, X. (2020). Describing the Full Pore Size

Distribution of Tight Sandstone and Analyzing the Impact of Clay Type on Pore Size Distribution. *Geofluids*. doi:10.1155/2020/5208129

Qu, Z. (1990). Bulk granularity division diagrams & their sedimentologic significance. *China Offshore Oil & Gas (Geology), 4*(3), 37-48+37-38.

Senlin, Y., Yukun, C., & Xiaojun, W. (2018). Different pore structure modalities in sandy conglomerate reservoirs and their forming mechanisms. *Arabian Journal of Geosciences*. doi:10.1007/s12517-018-3992-6

Sette, S., & Boullart, L. (2001). Genetic programming: Principles and applications. *Engineering Applications of Artificial Intelligence, 14*, 727-736. doi:10.1016/S0952-1976(02)00013-1

Visher, G. (1969). Grain Size Distributions and Depositional Processes. *Journal of Sedimentary Research - J SEDIMENT RES, 39*(3), 1074-1106. doi:10.1306/74D71D9D-2B21-11D7-8648000102C1865D

Weichao, T., Shuangfang, L., Wenbiao, H., Shuping, W., Yang, G., Weiming, W., . . . Zhuochen, Z. (2019). Study on the Full-Range Pore Size Distribution and the Movable Oil Distribution in Glutenite. *Energy & Fuels*. doi:10.1021/acs.energyfuels.9b00999

Xiao, M., Wu, S., Yuan, X., Cao, Z., & Xie, Z. (2020). Diagenesis effects on the conglomerate reservoir quality of the Baikouquan Formation, Junggar Basin, China. *Journal of Petroleum Science and Engineering, 195*, 107599. doi:https://doi.org/10.1016/j.petrol.2020.107599

Xie, K., Lu, X., Li, Q., Jiang, W., & Yu, Q. (2016). Analysis of Reservoir Applicability of Hydrophobically Associating Polymer. *SPE Journal, 21*(01), 1-9. doi:10.2118/174553-PA

Yan, J., Fan, J., Wang, M., Li, Z., Hu, Q., & Chao, J. (2018). Rock fabric and pore structure of the Shahejie sandy conglomerates from the Dongying depression in the Bohai Bay Basin, East China. *Marine and Petroleum Geology, 97*, 624-638. doi:https://doi.org/10.1016/j.marpetgeo.2018.07.009

Yin, S., Chen, Y., & Wu, X. (2018). Different pore structure modalities in sandy conglomerate reservoirs and their forming mechanisms. *Arabian Journal of Geosciences, 11*(21), 654. doi:10.1007/s12517-018-3992-6

Yin Senlin, C. G., Chen Yukun, Wu Xiao jun. (2019). Mechanism of complex modes of the pore structure of sandstone/conglomerate reservoirs. *Journal of Southwest petroleum university (Science & Technology Edition), 41*(1), 1-17. doi:10.11885/j.issn.1674-5086.2018.01.01.01

Zhai, H., Xue, Z., Park, H., Aizawa, Y., Baba, Y., & Zhang, Y. (2020). Migration characteristics of supercritical CO2 microbubble flow in the Berea sandstone revealed by voxel-based X-ray computed tomography imaging analysis. *Journal of Natural Gas Science and Engineering, 77*, 103233. doi:https://doi.org/10.1016/j.jngse.2020.103233

Zhang, C., Song, X., Wang, X., Wang, X., Zhao, K., Shuang, Q., & Li, S. (2020). Origin and depositional characteristics of supported conglomerates. *Petroleum Exploration and Development, 47*(2), 292-305. doi:https://doi.org/10.1016/S1876-3804(20)60047-7

Zhang, K., Wu, S., Zhong, Y., & Shi, L. (2020). Modal distribution of pore-throat size in sandy conglomerates from an alluvial fan environment: Lower Karamay Formation, Junggar Basin, West China. *Marine and Petroleum Geology, 117*, 104391. doi:https://doi.org/10.1016/j.marpetgeo.2020.104391

Zhao, F., Hao, H., Lv, G., Wang, Z., Hou, J., Wang, P., . . . Li, W. (2018). Performance improvement of CO2 flooding using production controls in 3D areal heterogeneous models: Experimental and numerical simulations. *Journal of Petroleum Science and Engineering, 164*, 12-23. doi:https://doi.org/10.1016/j.petrol.2018.01.036

Zhao, Y., Zhu, G., Dong, Y., Danesh, N. N., Chen, Z., & Zhang, T. (2017). Comparison of low-field NMR and microfocus X-ray computed tomography in fractal characterization of pores in artificial cores. *Fuel, 210*, 217-226. doi:https://doi.org/10.1016/j.fuel.2017.08.068

Zheng Mingming, J. G., Liu Zhichao, Liu Tianle, Peng Li, Wang Zhen, Cao Han, Sun Pinghe. (2016).

Experimental research on artificial long core technology with predesigned physical parameters. *Geologicall Science and Technology Information, 35*(6), 222-229.